JOURNAL OF PETROLOGY | VOLUME 41 | NUMBER 5 | PAGES 717–737 | 2000

Silicic Magma Formation in Overthickened Crust: Melting of Charnockite and Leucogranite at 15, 20 and 25 kbar

BORIS A. LITVINOVSKY[1], IAN M. STEELE[2] AND STEPHEN M. WICKHAM[2]*

[1]GEOLOGICAL INSTITUTE, SIBERIAN DEPARTMENT OF THE RUSSIAN ACADEMY OF SCIENCES, 6A SAKHYANOVA STR., ULAN-UDE 670047, RUSSIA

[2]DEPARTMENT OF GEOPHYSICAL SCIENCES, UNIVERSITY OF CHICAGO, 5734 SOUTH ELLIS AVENUE, CHICAGO, IL 60637, USA

RECEIVED JUNE 4, 1997; REVISED TYPESCRIPT ACCEPTED NOVEMBER 2, 1999

Two models of silicic magma formation have been experimentally tested: (1) generation of A-type granite magma by partial melting of crustal source rocks at depths >50 km; (2) production of syenite magma by partial melting of quartzofeldspathic rocks at pressures >15 kbar. Melting experiments at 15, 20 and 25 kbar were performed on Archaean biotite-bearing charnockite of opx-bearing granodiorite composition, and on leucogranite. Most experiments were conducted with oxalic acid (OA) to provide 2 wt % H_2O and ~3 wt % CO_2, but several fluid-absent runs with charnockite were also made. The temperature interval of the OA experiments was ~925–1100°C; for the dry runs it was ~1100–1250°C. In all cases, melting reactions produced garnet (Grt), clinopyroxene (Cpx), ternary feldspar (Tfsp) and 5–85 vol. % melt. The composition of partial melts produced from charnockite for degrees of melting up to ~60 vol. % is always granitic and is controlled by residual Tfsp and Qtz. Ternary feldspar acts as a sink for alkalis until totally consumed at ~50 vol. % melting. The granitic composition of the initial melt results from incongruent melting of natural silicic rocks, and contrasts with the haplogranitic system Ab–Or–Qtz in which the initial melt is generally considered to be of syenitic composition at these high pressures. The presence of Ca-, Mg- and Fe-bearing phases in many natural rocks defines peritectic melting reactions that result in the formation of the low-silica phases Grt and Cpx together with partial melt. The resulting SiO_2 enrichment in the partial melt prevents the formation of syenitic liquids by partial melting of quartzofeldspathic rocks, even at very great depth. The predominance of Grt and Cpx in the residue at ~50 vol. % partial melting may promote separation of granite magma from restite by settling of these denser minerals. High degrees of melting of ~50–60 vol. %, accompanied by settling of residual crystals, would lead to a magma of restricted compositional range with a heavy rare earth element depleted pattern. Overall, the granitic melt composition obtained in the experiments differs from that of A-type granite. However, at degrees of melting below ~30%, the composition of partial melt resembles A-type granite although its Al_2O_3 content is more than 1 wt % higher.

KEY WORDS: *high-pressure melting experiments; melting of charnockite; A-type granite; syenite magma; deep-crustal melting*

INTRODUCTION

Various observations suggest that some quartzofeldspathic rocks have been metamorphosed and possibly melted at great depth characteristic of the deeper parts of overthickened crust or even uppermost mantle. The evidence includes: (1) coesite-bearing gneiss (Schreyer *et al.*, 1987; Schreyer, 1988); (2) high-pressure (up to 15–20 kbar) granulites (Grew, 1984; Sandiford & Powell, 1986; Pin & Vielzeuf, 1988; Harley, 1989; Barbey *et al.*, 1990; see also references in Vielzeuf & Holloway, 1988, p. 272); (3) the presence of silicic rocks associated with basaltic eclogites (Sobolev *et al.*, 1986; Black *et al.*, 1988;

*Corresponding author. Present address: Galson Sciences Ltd, 5, Grosvenor House, Melton Road, Oakham LE15 6AX, UK.

Schliestedt & Okrusch, 1988; Schertl *et al.*, 1991; Schmidt, 1993; Snoeyenbos & Williams, 1994; Zhang *et al.*, 1994). It is possible that if deeply submerged crustal blocks are underplated or intruded by basalt magma, the silicic material would be subjected to partial melting. As crustal blocks lose water during tectonic burial, and pressure at subcrustal depths is typically >15 kbar, significant partial melting of silicic rocks would occur only at fairly high temperature, ~950°C or even higher (Stern *et al.*, 1975). There is evidence that temperatures as high as this may be attained in some high-pressure granulite terranes (Hayob *et al.*, 1989). Depending on the source rock composition, two different types of silicic magmas, essentially sodic (Na > K) or potassic (K > Na), can be produced. Generation of Na-rich silicic melts at 15 kbar was experimentally studied by many researchers (Huang & Wyllie, 1986; Johnston & Wyllie, 1988; Carroll & Wyllie, 1990). It is of interest to define the composition of melts formed at high pressure by partial melting of K-rich source rocks because some aspects of the melting conditions (low water content and high temperatures) are typical of A-type granites (Clemens *et al.*, 1986; Litvinovsky, 1990; Vielzeuf *et al.*, 1990).

Several hypotheses have been proposed for the formation of A-type granitoid magmas. A fundamental problem is whether A-type granitoids are exclusively crustal derived (e.g. Clemens *et al.*, 1986; Vielzeuf *et al.*, 1990; Rämö, 1991; Anderson & Morrison, 1992), or require significant mixing between components derived from both the mantle and crust coupled with fractionation processes (e.g. Barker *et al.*, 1975; Wickham *et al.*, 1995), or whether they form by fractional crystallization of basalt magma. There is further dispute between those who argue for an origin by partial melting of already melt-depleted granulite (Clemens *et al.*, 1982; Vielzeuf *et al.*, 1990) and those who argue for partial melting of non-restitic meta-igneous tonalitic to granodioritic crust that has not necessarily been melt depleted but may have been partly dehydroxylated (Creaser *et al.*, 1991; Rämö, 1991; Anderson & Morrison, 1992; Skjerlie & Johnston, 1993). Melting experiments on silicic rocks at P and T conditions corresponding to high granulite and eclogite metamorphic grades may provide evidence for A-type granite magma generation at great depth from crustal source rocks.

Such experiments also have a bearing on the syenite problem. According to melting experiments performed in the system Ab–Or–Qtz ($\pm$ H_2O) by Huang & Wyllie (1975, 1981), Johannes & Holtz (1990) and Ebadi & Johannes (1991), the composition of the initial melt (eutectic or cotectic) becomes progressively richer in the albite component as pressure increases, irrespective of the water content of the system. In other words, the initial melt becomes less granitic and more syenitic. All the above experiments were performed at pressures of 15 kbar or less. Huang & Wyllie (1975) compiled available data for the system Ab–Or–Qtz ($\pm$ H_2O), and constructed field boundaries at 20 and 30 kbar showing that at pressures exceeding 20 kbar, the initial melt composition is syenitic. These workers assumed that some syenite melts could be generated by partial melting of silicic source rocks at the base of an overthickened crust (Huang & Wyllie, 1981). We have experimentally tested the conclusion of Huang & Wyllie (1975), which is based on a study of a haplogranite or Ab–Or–Qtz systems, by partial melting experiments using natural quartzofeldspathic rocks.

Many melting studies have been performed on metamorphic and igneous silicic rocks at normal crustal P–T conditions (up to 10 kbar), but only a few have been conducted on silicic rocks at pressures representative of the base of thickened continental crust or to uppermost mantle in regions of plate convergence. Of the latter, most experiments have been performed on tonalite and trondhjemite compositions, as indicated above; low-potassium silicic melts were generated (Huang & Wyllie, 1986; Johnston & Wyllie, 1988; Carroll & Wyllie, 1990). High-potassium silicic melts were obtained in a few high-pressure experiments (from 13 to 20 kbar) on quartzofeldspathic rocks (Patiño Douce & Johnston, 1991; Skjerlie & Johnston, 1993, 1996). Quartzofeldspathic rocks are voluminous in many granulite terranes (Grew, 1984; Petrova & Levitsky, 1984; Harley, 1989; Vielzeuf *et al.*, 1990) and can be regarded as a potentially significant source of K-rich granitic melts if subducted to high pressure and temperatures in collision or subduction zones (Schreyer *et al.*, 1987).

We have performed melting experiments on charnockite (opx-bearing granodiorite composition) at 15, 20 and 25 kbar, both under fluid-absent conditions and with an H_2O–CO_2 fluid phase present. In addition, several experiments were performed on a leucogranite bulk composition. The main goals of the studies were to establish the following: (1) whether partial melting of ordinary quartzofeldspathic crustal rocks at high pressure can result in production of syenitic melt; (2) if the partial melt is of granitic composition, does it correspond to an A-type granite? In accordance with these goals we determined: (1) the composition of melts as a function of T and $P \pm$ H_2O–CO_2; (2) the possible correlation of melt composition with the extent of melting; (3) the mineralogical composition of the residual crystal phases (subliquidus minerals); (4) the partial melting reactions.

CHARACTERIZATION OF STARTING MATERIAL AND EXPERIMENTAL CONDITIONS

The experiments were performed in the Experimental Petrology Laboratory in the Department of Geophysical

Sciences at the University of Chicago. Most experiments were conducted mainly on an Archaean charnockite from the Sharyzhalgai metamorphic massif exposed near the southwestern end of Lake Baikal (Petrova & Levitsky, 1984). Samples were kindly provided by Professor Z. Petrova. Silicic granulites, metamorphosed under middle- and lower-crustal conditions, are abundant in the Sharyzhalgai massif and vicinity, and these rocks can be regarded as possible source rocks for Palaeozoic granites and syenites occurring throughout Transbaikalia and North Mongolia (Zanvilevich *et al.*, 1985; Litvinovsky *et al.*, 1989; Wickham *et al.*, 1995).

The charnockite was chosen because its chemical composition corresponds approximately to the average composition of silicic granulites of the Sharyzhalgai massif (Petrova & Levitsky, 1984). We also performed several melting experiments on a leucogranite from Central Transbaikalia. The bulk compositions of the two starting materials along with the modal proportions and composition of minerals are given in Table 1.

It is often assumed that melting under granulite grade occurs in water-undersaturated conditions with prevalence of CO_2 over H_2O in the fluid phase if one is present (Collerson & Fryer, 1978; Newton *et al.*, 1980; Aranovich *et al.*, 1987; Touret, 1992; Andersen *et al.*, 1993; Litvinovsky & Podladchikov, 1993). Therefore we performed two groups of experiments including both fluid-absent and fluid-present conditions. In fluid-present runs, oxalic acid (OA) was added to give $\sim$2 wt % H_2O (and consequently 3·3 wt % CO_2). In addition, $\sim$0·8 wt % H_2O is present in biotite and hornblende. This provided water-undersaturated melting conditions.

Experiments were run at 15, 20 and 25 kbar, covering the temperature intervals 950–1075°C in fluid-present, and 1100–1225°C in fluid-absent systems. Some experiments were performed at 900°C, but did not contain discernible amounts of glass. Inasmuch as the purpose was to study the composition of melt produced by a relatively high degree of melting (>10%), we were not concerned with accurate determination of solidus and liquidus temperatures. Run conditions and phase assemblages are given in Table 2.

It is known that in fluid-absent experiments at high pressure, equilibrium is difficult to achieve, even after 3–4 weeks (Skjerlie & Johnston, 1993). In runs with oxalic acid we also did not achieve equilibrium, although run duration ranged from 1 day to 2 weeks. Samples from two runs of different duration (1 and 2 weeks) did not exhibit any significant difference in the proportion of relict quartz and plagioclase or in the composition of newly formed glass and crystals. For these reasons, most runs ranged from 7–8 days at the lowest temperatures to 3 days at the highest temperatures. Although complete equilibrium was not reached in the experiments, local equilibrium between melt and new crystals is suggested by systematic changes in the composition of both melt and crystal phases as a function of T and P (see below, Figs 4–8 and 13). In runs where the amount of glass did not exceed 10–15 vol. %, the compositions of glass and newly formed mafic minerals are uniform throughout the sample. In addition, compositions of euhedral feldspar crystals dispersed in the glass are very similar to the rims around feldspar grains (see below, Table 5 and Fig. 12), and this is taken as evidence of approach to equilibrium among the newly formed phases.

EXPERIMENTAL AND ANALYTICAL PROCEDURES

Samples of charnockite and leucogranite were crushed in a tungsten carbide shatter box and then ground by hand in an agate mortar under acetone to an average grain size of 10–20 mm with rare grains of biotite and plagioclase up to 40 mm. The powdered starting material was dried at 120°C and stored in a desiccator.

High-pressure experiments were performed in a piston-cylinder apparatus of 0·75 inch (19 mm) diameter with samples enclosed mostly in gold capsules to minimize Fe loss. For some runs performed at P–T conditions above the gold melting point, platinum capsules were used. Two types of solid-medium cell assemblies were used: (1) NaCl up to $\sim$30°C below the melting point of NaCl at a given pressure; (2) $BaCO_3$ at higher temperatures. To evaluate the influence of the capsule and the solid-medium cell materials on the chemical composition of the run products, we performed two parallel sets of runs, using gold and platinum capsules, and NaCl and $BaCO_3$ cell assemblies, at the same P and T. No significant difference between the run products was detected. Reported pressures incorporate no friction correction and are believed accurate to $\pm$5% of the quoted value. Temperature was measured with a $W_{75}Re_{25}/W_{97}Re_3$ thermocouple located $\sim$1 mm above the sample capsule and controlled to within $\pm$5°C of the set point by a digital, solid-state controller.

Each experimental run was sectioned and polished for optical and microprobe study. Detailed imaging and analysis of the run products were performed with a Cameca SX-50 electron microprobe at the University of Chicago. Two types of images proved useful: (1) backscattered electron (BSE) images allowed recognition of textures and mineralogy for most phases and were used to locate analysis positions; (2) panchromatic cathodoluminescence (CL) images showed subtle details of several phases including quartz, plagioclase and alkali feldspar. These details included overgrowths on quartz, zoning in some feldspars, and clear recognition of glass, which shows either no or very weak CL. Some of these phases are nearly indistinguishable on BSE images because of

Table 1: Characterization of the starting material

Rock or mineral	Modal proportion	SiO_2	TiO_2	Al_2O_3	FeO*	MnO	MgO	CaO	Na_2O	K_2O	Total
Charnockite, bulk rock[1]		67·10	0·30	15·03	4·52	0·04	1·80	3·20	3·91	2·90	99·63
Plagioclase	54	61·77	0·22	23·95	0·03	0·01	n.d.	5·75	8·09	0·22	100·04
Microcline	11	65·74	0·03	18·20	0·01	0·00	n.d.	n.d.	1·19	14·53	99·70
Biotite	14	36·40	3·37	14·90	21·24	0·09	9·13	n.d.	0·02	9·40	94·55
Amphibole	3	45·77	0·97	8·17	19·22	0·42	9·81	10·99	1·00	0·86	97·21
Orthopyroxene	3	50·90	0·09	0·49	32·81	1·83	13·49	0·85	n.d.	n.d.	100·46
Quartz	13										
Ap, Zir, pyrite	2										
Charnockite glass ($n = 4$)		66·81	0·35	15·21	5·00	0·05	1·73	3·70	3·85	2·83	99·53
Leucogranite[1]		74·62	0·22	13·58	1·63	0·09	0·13	0·79	4·24	4·71	100·64
Leucogranite glass ($n = 7$)		74·63	0·20	13·37	2·01	0·15	0·10	0·64	4·09	5·06	100·25

Chemical data in wt %; modal proportion in vol. % (point counting in large thin sections). Microprobe analyses of minerals are average of 3–7 crystals. FeO*, total Fe as FeO. n.d., not determined (here and in all the other tables).
[1]Analysed by 'wet ' chemistry; contents of P_2O_5 and LOI in charnockite are 0·14 and 1·01, respectively; in leucogranite these values are 0·12 and 0·51.

Table 2: Run conditions

Run	*P* (kbar)	*T* (°C)	Duration (day)	Dry (–); with OA (+)	Cell	Phase assemblage	Relict minerals
Charnockite							
37	25	950	11·5	+	NaCl	Grt, Cpx, Tfsp, Qtz, Gl [5]	Qtz, Pl
34	25	975	14	+	NaCl	Grt, Cpx, Tfsp, Gl [15]	Qtz, Pl, Kfs
24	25	1000	8·5	+	NaCl	Grt, Cpx, Tfsp, Qtz, Gl [30]	Qtz, Pl
5	25	1000	1	+	NaCl	Grt, Cpx, Tfsp, Gl [25]	Qtz, Pl, (Opx)
51	25	1025	7	+	NaCl	Grt, Cpx, Gl [50]	Qtz
41	25	1050	4	+	NaCl	Grt, Cpx, Gl [70]	Qtz
45	25	1075	3	+	NaCl	Grt, Gl [80]	
2	25	1100	1	—	NaCl	Grt, Cpx, Tfsp, Gl [5]	Pl, Qtz, (Opx)
4	25	1150	7	—	NaCl	Grt, Cpx, Tfsp, Gl [15]	Qtz, Pl, Kfs
10	25	1200	1	—	$BaCO_3$	Grt, Cpx, Tfsp, Mt, Gl [45]	Qtz, Pl, (Opx)
16	25	1225	2	—	$BaCO_3$	Grt, Cpx, Mt, Gl [70]	Qtz, Pl
23	20	950	7	+	NaCl	Grt, Cpx, TFSP, Gl [15]	Qtz, Pl, Kfs
40	20	1000	7	+	NaCl	Grt, Cpx, Qtz, Gl [50]	Qtz
11	20	1000	2·5	water*	NaCl	Grt, Qtz, Mt, Gl [70]	Qtz
49	20	1025	7	+	NaCl	Grt, Cpx, Gl [60]	Qtz
38	20	1050	4	+	NaCl	Grt, Cpx, Gl [70]	Qtz
53	20	1075	3	+	NaCl	Grt, (Cpx), Gl [85]	
8	20	1200	1	—	$BaCO_3$	Grt, Cpx, Tfsp, Gl [50]	Qtz, Pl
13	15	950	4	+	NaCl	Grt, Cpx, Tfsp, Gl [20]	Qtz, Pl, Kfs
48	15	975	5	+	NaCl	Grt, Cpx, Qtz, Gl [50]	Qtz, Pl
55	15	1000	5	+	NaCl	Grt, Cpx, Gl [60]	Qtz, Pl
54	15	1040	3	+	$BaCO_3$	Grt, (Cpx), Gl [70]	Qtz
56	16	1060	3	+	$BaCO_3$	Grt, (Cpx), Gl [90]	
25	15	1100	8·5	–	NaCl	Grt, Cpx, Qtz, Tfsp, Gl [10]	Qtz, Pl, (Kfs)
15	15	1150	5	–	$BaCO_3$	(Grt), Cpx, Qtz, Gl [75]	(Qtz)
Leucogranite							
22	25	950	7	+	NaCl	Grt, Cpx, Qtz, Tfsp, Mt, Gl [15]	Qtz, Pl, Kfs
18	25	1000	3·5	+	NaCl	Grt, Cpx, Qtz, Tfsp, Mt, Gl [40]	Qtz, Pl
19	25	1050	3	+	NaCl	Grt, Cpx, Qtz, Mt, Gl [80]	Qtz, Pl
17	20	1000	3·5	+	NaCl	Grt, (Cpx), Qtz, Mt, Gl [60]	Qtz, Pl

Grt, garnet; Cpx, clinopyroxene; Opx, orthopyroxene; Qtz, quartz; Pl, plagioclase; Tfsp, ternary feldspar; Kfs, K-feldspar; Mt, magnetite; Gl, glass. Symbols in parentheses indicate trace amount of mineral phase. Numbers in brackets are estimated vol. % of glass.
*2 wt % of pure H_2O.

their very similar average atomic number but the CL image often showed clear contrast. Simultaneous observation of BSE and CL images allowed all phases to be recognized and analysis positions accurately located on the phases of interest (Fig. 1a and 1b; see also Fig. 10, below). In some special cases, we used CaK_α X-ray images, as they proved useful in distinguishing glass and various crystal phases (Fig. 1c).

All analyses were made using wavelength-dispersive spectrometers, 15 kV accelerating voltage, and either 10 or 25 nA beam current. For garnet and pyroxene, a focused beam was used, whereas for glass and feldspar the beam was rastered at a scale sufficient to include only the phase of interest in the scanned area (from 2 to 10 mm on a side) as observed using the BSE and CL image. The accuracy of this procedure was confirmed by analysing a totally melted run, which allowed comparison of the analysis of the starting material with the resulting microprobe analysis (Table 1). Some phases, especially pyroxene, were usually <5 mm in size. Con-

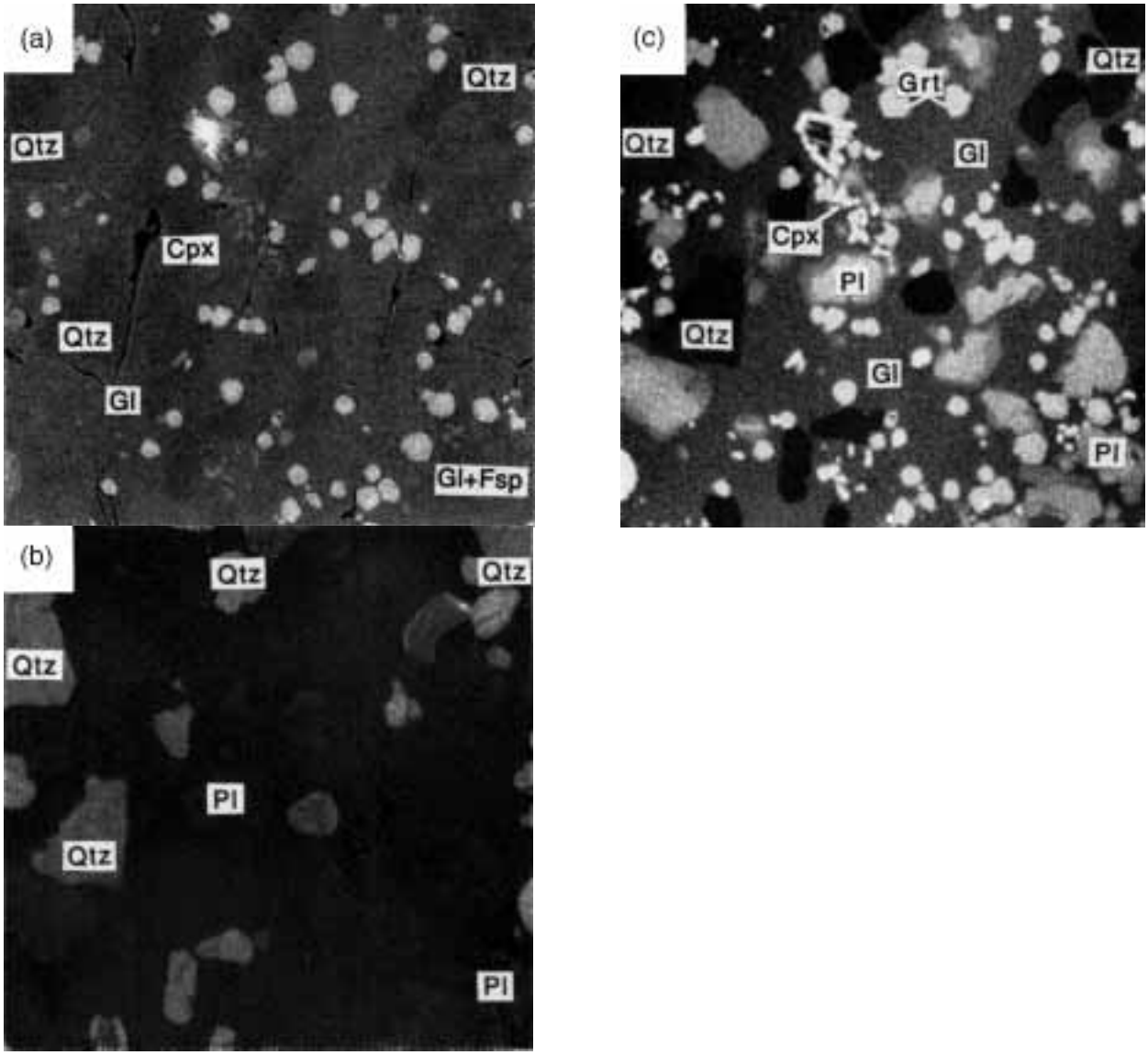

Fig. 1. Digital images of the polished surface of a run product at 25 kbar, 1200°C, water-absent conditions. (a) Back-scattered electron (BSE) image; (b) cathodoluminescence (CL); (c) CaK_{α} X-ray. Width of fields of view 250 mm. Each image emphasizes different aspects of the same sample and some phases are indicated (Grt, garnet; Qtz, quartz; Cpx, clinopyroxene; Gl, glass; Fsp, feldspar; Pl, plagioclase).

tamination of the analytical volume is therefore possible, and stoichiometry was used to eliminate suspect data. Using four spectrometers, the volatile elements (Na and K) were analysed first. Significant loss of sodium occurred only in very small, about 3–5 mm, areas of glass (see Tables 3 and 4).

Determination of the amount of melt and minerals was difficult, especially in the low-temperature charges. Point counting in transparent light was not possible, as the grain size was less than section thickness. Mass balance calculations were not accurate because of the abundance of zoned relict minerals. In many samples the glass distribution is uneven and representative photomosaics were difficult to obtain. Precise determination of glass and crystal proportion was not our main purpose, and the melt fraction was estimated from optical study and point counting of sections. Although uncertain, this method allows relative estimates of glass from run to run as a function of temperature. The accuracy of about ± 5 vol. % is satisfactory, as the melt proportion ranges from some few percent to almost 100%. Numbers in brackets in Table 2 correspond to this estimate.

Table 3: Chemical composition of experimental products; starting material charnockite, with oxalic acid

	SiO_2	TiO_2	Al_2O_3	FeO*	MnO	MgO	CaO	Na_2O	K_2O	Total
15 kbar and 950°C										
Gl	72·90	0·35	14·65	1·82	0·00	0·21	0·92	3·80	5·35	95·69
Grt	38·65	1·62	20·08	24·60	n.d.	6·97	6·74	0·14	0·01	98·81
Cpx	52·66	0·30	8·62	10·67	0·09	10·00	13·85	2·03	0·13	98·35
15 kbar and 975°C										
Gl	72·61	0·40	14·87	1·64	0·05	0·42	1·50	4·32	4·19	94·54
Grt	39·21	1·69	20·78	23·44	0·45	7·43	6·54	0·07	0·03	99·64
Cpx	51·53	0·43	6·61	10·38	0·12	11·61	16·57	1·30	0·03	98·58
15 kbar and 1000°C										
Gl	72·97	0·31	14·65	1·45	0·04	0·45	2·00	4·23	3·90	93·58
Grt	38·86	1·31	20·79	22·00	0·52	8·24	7·48	0·07	0·02	99·29
Cpx	50·71	0·59	7·84	10·75	0·14	11·56	15·68	1·41	0·06	98·74
15 kbar and 1040°C										
Gl	72·36	0·36	14·92	1·66	0·01	0·48	2·06	4·00	4·15	93·12
Grt	39·44	0·93	20·97	19·99	0·61	10·37	7·21	0·03	0·01	99·56
Cpx	51·70	0·36	6·99	10·41	0·19	12·66	14·65	1·35	0·06	98·37
15 kbar and 1060°C										
Gl	73·14	0·32	14·14	1·64	0·02	0·55	2·16	4·23	3·80	93·73
Grt	39·62	0·93	20·73	20·05	0·54	10·18	7·20	0·05	0·03	99·33
Cpx	51·94	0·40	7·39	9·46	0·14	12·45	17·06	1·59	0·12	100·55
20 kbar and 950°C										
Gl	73·11	0·11	15·15	1·02	0·20	0·11	0·86	1·54[1]	3·22[1]	95·32
Grt	38·31	1·05	20·34	24·72	0·49	7·17	7·46	0·04	0·07	99·65
Cpx	52·66	0·30	10·32	8·67	0·09	10·00	12·85	2·73	0·13	99·75
20 kbar and 1000°C										
Gl	73·19	0·28	15·02	0·89	0·03	0·32	1·74	4·37	4·16	94·00
Grt	39·55	1·61	20·67	21·23	0·43	8·85	6·85	0·12	0·03	99·34
Cpx	52·47	0·72	10·32	7·49	0·11	10·26	15·66	2·78	0·06	99·87
20 kbar and 1000°C (2 wt % pure water)										
Gl	69·52	0·48	16·59	1·46	0·00	1·39	2·58	4·35	3·63	96·37
Grt	37·99	2·50	20·30	22·02	0·40	12·59	2·94	0·10	0·02	98·86
Cpx	51·60	0·22	8·63	10·41	0·10	13·63	12·56	1·94	0·04	99·13
20 kbar and 1025°C										
Gl	72·18	0·28	15·65	0·93	0·01	0·38	2·17	4·38	4·02	93·04
Grt	39·70	1·55	20·73	21·04	0·44	8·49	7·33	0·11	0·03	99·42
Cpx	50·99	0·51	9·44	8·63	0·14	10·84	15·51	2·30	0·08	98·44
20 kbar and 1050°C										
Gl	71·73	0·28	14·47	1·55	0·03	0·44	2·09	4·93	4·48	94·41
Grt	39·97	1·40	21·15	20·95	0·42	8·69	6·93	0·14	0·02	99·67
Cpx	50·65	0·76	9·35	8·94	0·11	11·11	15·45	3·25	0·05	99·67
20 kbar and 1075°C										
Gl	71·57	0·33	15·00	1·81	0·02	0·61	2·19	5·02	3·45	93·71
Grt	38·95	1·27	21·17	20·21	0·50	9·33	7·24	0·08	0·04	98·79
Cpx	51·12	0·36	7·53	8·09	0·13	12·15	17·52	1·79	0·03	98·72
25 kbar and 950°C										
Gl	72·93	0·26	15·21	0·91	0·01	0·13	1·33	4·26	4·96	94·15
Grt	39·73	1·15	20·64	22·99	0·41	6·82	8·46	0·17	0·02	100·39
Cpx	53·07	0·67	14·70	6·81	0·06	5·71	12·02	5·76	0·06	98·86

Table 3: continued

	SiO_2	TiO_2	Al_2O_3	FeO*	MnO	MgO	CaO	Na_2O	K_2O	Total
25 kbar and 975°C										
Gl	72·59	0·21	15·25	1·17	0·01	0·07	0·82	4·72	5·16	93·87
Grt	38·86	1·06	21·05	23·36	0·41	7·03	7·53	0·27	0·02	99·59
Cpx	53·37	0·66	15·77	7·53	0·08	5·80	10·75	5·96	0·06	99·98
25 kbar and 1000°C (Run 24)										
Gl	73·04	0·33	15·55	1·27	0·02	0·09	0·91	3·79	5·00	94·41
Grt	38·63	1·11	21·08	23·69	n.d.	7·24	7·46	0·22	0·02	99·45
Cpx	52·37	0·61	14·75	8·83	0·13	6·25	11·94	5·02	0·06	99·96
25 kbar and 1000°C (Run 5)										
Gl	72·57	0·29	14·99	1·18	0·00	0·18	1·06	3·79	5·94	95·61
Grt	39·26	1·04	21·54	24·07	n.d.	7·17	7·38	0·19	0·02	100·67
Cpx	53·01	0·59	11·70	8·37	n.d.	7·43	14·84	4·46	0·17	100·57
25 kbar and 1025°C										
Gl	72·83	0·26	15·36	0·99	0·04	0·44	2·06	4·31	3·71	93·35
Grt	39·54	0·97	20·69	21·20	0·38	7·50	8·35	0·15	0·02	98·80
Cpx	52·37	0·66	12·13	6·17	0·07	8·36	15·47	3·50	0·05	98·78
25 kbar and 1050°C										
Gl	72·12	0·31	15·11	1·23	0·06	0·42	2·08	4·56	4·11	93·17
Grt	39·94	1·48	20·95	21·55	0·35	7·65	8·41	0·16	0·03	100·52
Cpx	52·30	0·53	13·66	6·83	0·05	8·12	15·32	3·79	0·04	100·64
25 kbar and 1075°C										
Gl	73·09	0·31	14·26	1·61	0·03	0·75	2·58	3·94	3·43	92·41
Grt	40·30	1·09	21·72	20·84	0·45	8·81	8·18	0·13	0·03	101·55

*All Fe expressed as FeO.
[1]Loss of both Na and K suspected because of very small areas of glass.
All data as wt %. Each analysis is the average of 3–5 analyses of different grains or glass (melt) areas. Totals listed are original totals of microprobe analyses; for glass analyses only, individual values are adjusted by normalization to total 100% to give a 'volatile-free' composition. The ternary feldspar compositions are given in Table 5.

EXPERIMENTAL RESULTS

Experimental conditions and resulting phase assemblages are summarized in Table 2 and Fig. 2. Although experiments were performed over a wide P–T range, the melting reactions always resulted in the assemblage garnet (Grt), clinopyroxene (Cpx), ternary feldspar (Tfsp) and glass. In some fluid-absent runs on charnockite and in runs with leucogranite + OA, accessory magnetite also formed. Unreacted quartz persisted in most runs and as this mineral was involved in melting reactions up to 80 vol. % melting, both relict resorbed grains and euhedral quartz crystals are sometimes present. For this reason quartz is shown in Table 2 as both a relict mineral and a reaction product. For the total of 29 runs, the most representative series of experiments was performed in the system charnockite–oxalic acid (see Fig. 2) and these are the basis for most descriptions and conclusions.

Both in fluid-absent and fluid-present systems the solidus-to-liquidus interval for charnockite is ~150°C. Mafic minerals of the starting material do not persist above near-solidus temperatures (when the proportion of glass is >5%), but rather react to form Grt and Cpx. In Fig. 3a, fluid-absent melting of charnockite resulted in small pools of melt around a fine-grained aggregate of Grt replacing flakes of biotite. Usually, glass is colourless, but in places it is dark brown immediately adjacent to the garnet and changes to colourless away from the garnet. The major element composition of glass remains constant irrespective of colour change, and colour variation probably represents variation in the iron oxidation state. Thin-section study shows that relict Pl and Qtz grains adjacent to melt are resorbed, suggesting their involvement in melting reactions. In all runs at ~10–15 vol. % melting, rims of Tfsp around the Pl grains are discernible, and amphibole and orthopyroxene are totally replaced by euhedral crystals of Grt and Cpx (see below, Fig. 8a and b). In runs with oxalic acid (Fig. 3b), pools of melt as well as grains of Grt, Cpx and Tfsp

Table 4: Chemical composition of experimental products; starting material charnockite (water-absent melting) and leucogranite (melting with the oxalic acid)

	SiO_2	TiO_2	Al_2O_3	FeO*	MnO	MgO	CaO	Na_2O	K_2O	Total
Charnockite										
15 kbar and 1100°C										
Gl	70·71	0·83	15·24	2·44	0·05	0·76	1·87	2·77[1]	5·33	97·45
Grt	38·95	1·65	20·73	20·96	n.d.	12·21	4·36	0·12	0·03	99·01
Cpx	51·38	0·72	7·33	10·75	0·21	12·02	14·51	2·08	0·04	99·04
15 kbar and 1150°C										
Gl	71·54	0·45	14·07	1·90	n.d.	1·55	2·82	3·90	3·77	96·65
20 kbar and 1200°C										
Gl	70·02	0·42	15·47	1·91	n.d.	0·96	2·27	4·04	4·88	96·74
Grt	38·51	1·19	20·82	22·05	n.d.	10·37	6·45	0·07	0·04	99·50
Cpx	52·56	0·41	9·04	7·13	n.d.	12·81	15·04	2·18	0·10	99·27
25 kbar and 1100°C										
Gl	69·45	0·87	14·95	3·36	0·02	0·47	1·39	3·95	5·54	96·25
Grt	38·61	2·29	20·60	22·78	0·44	8·38	6·24	0·30	0·03	99·67
Cpx	51·82	0·89	11·69	10·33	0·16	7·25	12·64	4·16	0·07	99·01
25 kbar and 1150°C										
Gl	71·32	0·51	14·63	2·90	n.d.	0·32	1·28	3·57	5·47	97·64
Grt	38·90	0·85	21·18	25·32	n.d.	5·02	9·32	0·17	0·02	100·78
Cpx	53·20	0·69	12·29	8·94	n.d.	6·77	12·22	5·58	0·08	99·77
25 kbar and 1200°C										
Gl	72·29	0·35	14·85	1·71	n.d.	0·18	1·13	4·09	5·40	95·56
Grt	38·54	1·78	20·82	23·00	n.d.	8·46	6·90	0·09	0·03	99·62
Cpx	50·16	0·62	10·40	11·02	n.d.	9·65	13·96	3·00	0·04	98·85
25 kbar and 1225°C										
Gl	69·96	0·45	15·84	1·52	n.d.	1·18	2·74	4·13	4·18	99·75
Grt	39·85	0·32	22·81	13·92	n.d.	13·81	8·06	0·03	0·01	98·81
Cpx	52·09	0·43	14·14	4·23	n.d.	10·24	14·58	3·45	0·07	99·23
Leucogranite										
20 kbar and 1000°C										
Gl	72·88	0·22	14·58	1·69	n.d.	0·10	0·61	4·46	5·46	95·00
Grt	38·64	1·30	19·44	26·88	1·50	3·96	6·39	0·18	0·01	98·30
25 kbar and 950°C										
Gl	72·59	0·10	15·00	1·56	n.d.	0·01	0·44	4·48	5·82	92·53
Grt	37·31	0·50	19·60	32·33	1·45	1·64	6·15	0·31	0·07	99·36
Cpx	54·10	0·19	16·57	12·65	0·81	2·40	5·76	8·02	0·01	100·51
25 kbar and 1000°C										
Gl	72·20	0·32	15·25	1·35	n.d.	0·07	0·60	4·59	5·62	93·95
Grt	38·76	1·10	19·60	28·49	0·90	2·89	6·44	0·27	0·01	98·46
Cpx	53·88	0·59	13·87	12·03	1·00	2·99	7·80	6·88	0·13	99·17
25 kbar and 1050°C										
Gl	72·52	0·27	14·62	1·50	n.d.	0·07	0·58	4·64	5·80	93·72
Grt	39·83	1·20	18·30	29·84	1·10	3·40	5·23	0·27	0·10	99·27
Cpx	53·52	0·63	13·27	12·99	0·90	3·15	7·10	6·81	0·26	98·63

*All Fe expressed as FeO.
All data as wt %. Each analysis is the average of 3–5 analyses of different grains or glass (melt) areas. Totals listed are original totals of microprobe analyses; for glass analyses only, individual values are adjusted by normalization to total 100% to give a 'volatile-free' composition. The ternary feldspar compositions are given in Table 5.
[1]The sodium total for this sample is low due to loss of sodium during analysis.

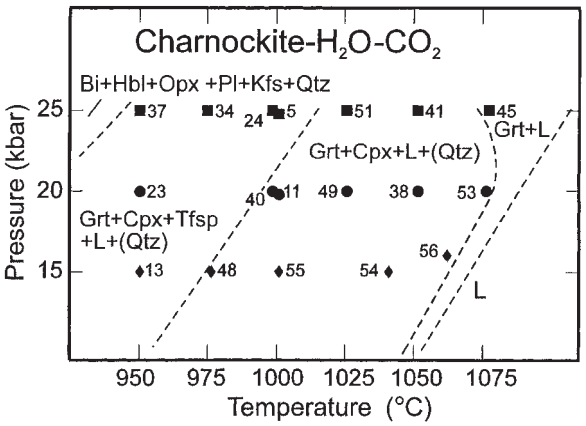

Fig. 2. Pressure–temperature conditions for runs involving charnockite with 2 wt % H_2O and 3·3 wt % CO_2 added in the form of oxalic acid. Different symbols are used for the three pressures and the numbers adjacent to the symbols indicate the run number. Approximate phase boundaries are indicated by the dashed lines.

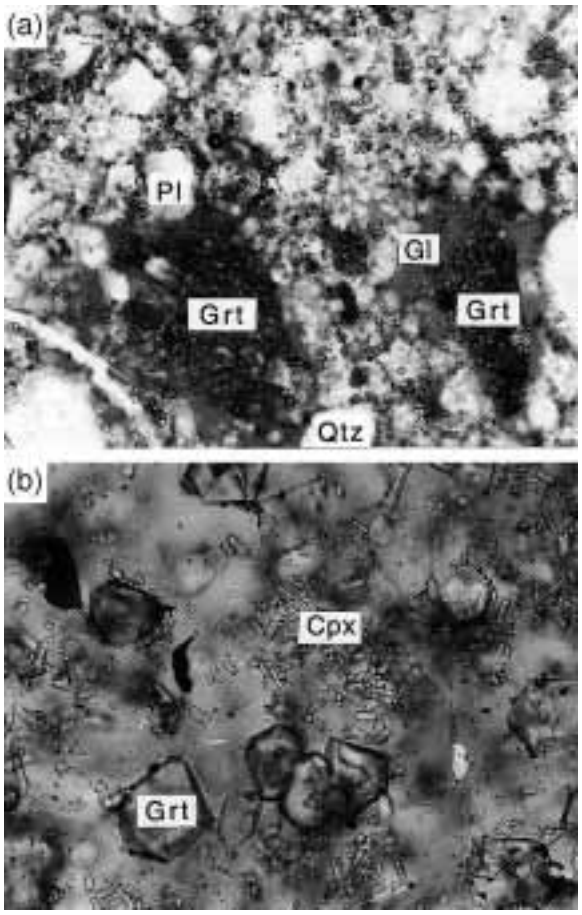

Fig. 3. Photomicrographs of charnockite at an early stage of melting. Transmitted light. The long axes of the photographs represent distances of 0·55 mm and 0·30 mm, respectively. (a) Water-absent melting, 15 kbar, 1100°C: pools of melt (grey) around and near the garnet aggregates are pseudomorphic after biotite flakes. (b) Run with H_2O and CO_2, 25 kbar, 975°C: garnet and clinopyroxene crystals as well as small pools of glass are evenly distributed throughout the sample.

are relatively evenly distributed in samples even in runs where the melt fraction was only ~10 vol. %. Relicts of initial mafic minerals are absent; and there are no pseudomorphic Grt aggregates with biotite morphology, as was observed in water-absent runs (Fig. 3a). These observations suggest that it was mainly addition of a free fluid phase, rather than the biotite breakdown reaction, that induced melting. In experiments on charnockite, Tfsp grains disappear at ~50 vol. % melting, Cpx remains until the melt proportion reaches 80–85%, and Grt is the only liquidus mineral (Fig. 2).

In four experiments on leucogranite (Table 4) the proportion of glass ranged from 15 to 80 vol. %. Grt, Cpx, Tfs and Mt formed as crystalline products of melting reactions, with Tfs disappearing in runs with 60 and 80% Gl. This suggests that the sequence of melting reactions in leucogranite was similar to that in charnockite.

Phase compositions

Garnet is formed in the melting reactions and is present in all runs (Table 2). Garnet composition is given in Tables 3 and 4. In Fig. 4 compositional variation of Grt as a function of T and P is shown, and in Fig. 5 the Grt compositions in melting experiments are plotted in the grossular–almandine–pyrope triangle. Garnets crystallizing in experiments with charnockite are characterized by a narrow range of composition as a function of pressure both in fluid-present and fluid-absent runs. Some trends are apparent: (1) garnet in the 25 kbar runs is richer in CaO and FeO, and depleted in MgO in comparison with garnets formed at 15 and 20 kbar; (2) at all pressures, a temperature rise results in the increase of MgO and consequent decrease of FeO*(FeO*is all Fe calculated as FeO) as seen by the increase in pyrope (Fig. 5); (3) pressure increase does not affect significantly the modal composition of Grt; only a slight increase in grossular is seen (Fig. 5). Garnet compositions differ between charnockite and leucogranite (see Tables 3 and 4, and Fig. 5), which reflects the compositional difference of starting materials.

Clinopyroxene forms tiny euhedral prisms that are closely associated with ternary feldspar grains replacing Pl at low extents of melting; in some areas feldspar grains are crowded with Cpx prisms (see Fig. 8, below). When the melt proportion exceeds 15–20 vol. %, Cpx crystals are relatively evenly distributed within the melt. The amount of Cpx decreases to zero when the proportion of melting is ~85 vol. %. Analysis of pyroxene compositional data (Tables 3 and 4) and diagrams (Figs 6

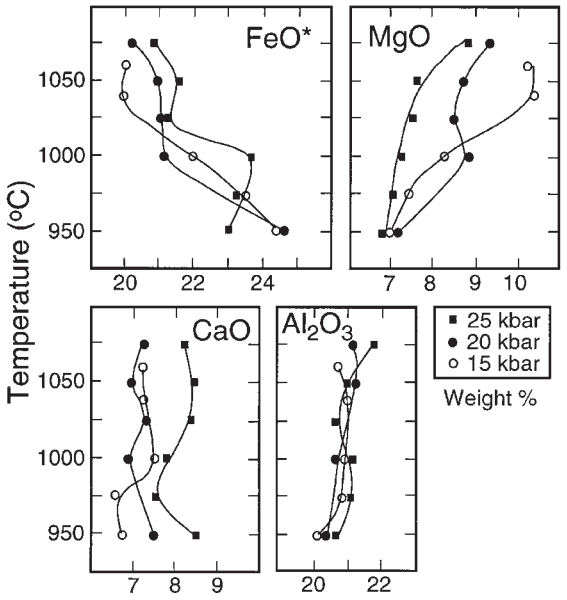

Fig. 4. Compositional variation of the experimentally produced garnet in the charnockite–H_2O–CO_2 system as a function of temperature and pressure. Total Fe given as FeO*.

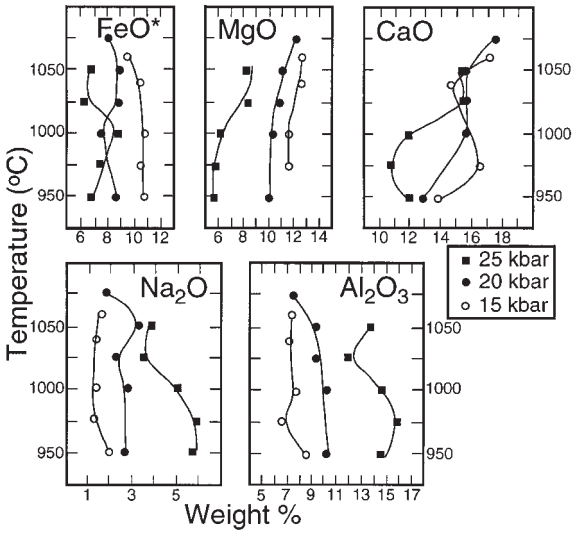

Fig. 6. Compositional variation of experimentally produced clinopyroxene in charnockite–H_2O–CO_2 system as a function of temperature and pressure.

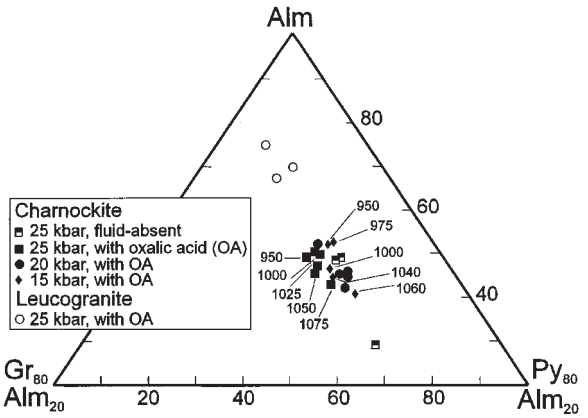

Fig. 5. Garnet compositions in melting experiments with charnockite and leucogranite plotted in the grossular–almandine–pyrope (Gr–Alm–Py) triangle. Temperatures at which garnets were grown are indicated.

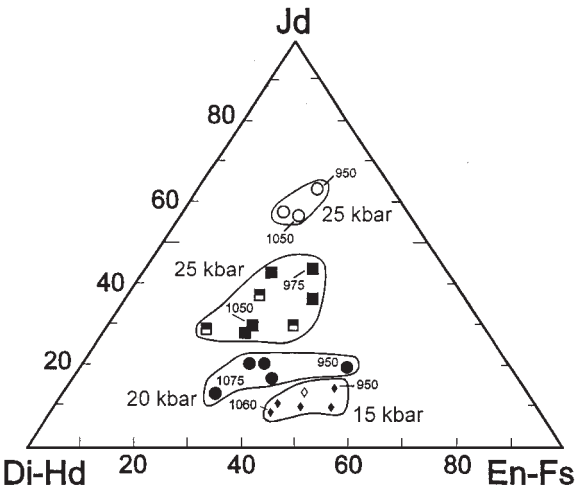

Fig. 7. Pyroxene compositions in melting experiments with charnockite and leucogranite plotted in the (Di–Hd)–Jd–(En–Fs) triangle [(diopside + hedenbergite)–jadeite–(enstatite + ferrosilite)]. Symbols as in Fig. 5. Temperatures at which pyroxenes were grown are indicated.

and 7) shows that pyroxenes crystallized at a given pressure exhibit only small differences in composition over a broad range of temperature although a small increase in MgO and CaO with rise in temperature can be seen (Fig. 6). Like garnets, pyroxene that crystallized at 25 kbar clearly differs from pyroxenes formed at 15 and 20 kbar. Whereas the lower-pressure pyroxenes are similar, the highest-pressure pyroxenes contain less MgO, CaO and FeO*. The largest difference is in Na_2O and Al_2O_3 (the jadeite component). This component systematically increases with pressure and shows a tendency to an inverse correlation with temperature (Figs 6 and 7). The pyroxene composition in fluid-absent and fluid-present melting experiments with charnockite is very similar at the same pressures (Fig. 7). However, pyroxenes crystallized at 25 kbar in the systems charnockite–H_2O–CO_2 and leucogranite–H_2O–CO_2 differ significantly in composition. The higher jadeite component in Cpx of leucogranite is apparently caused by the higher proportion of Na_2O + Al_2O_3 relative to CaO + MgO + FeO*in the starting material (Table 1).

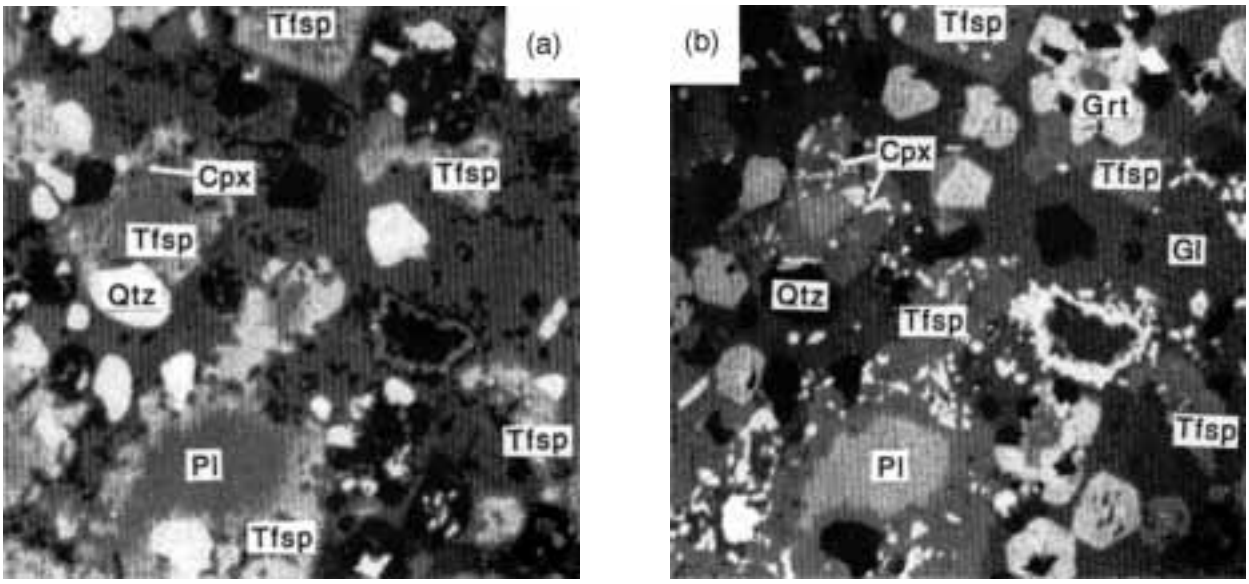

Fig. 8. Ternary feldspar (Tfsp) euhedral crystals and rims around plagioclase in CL (a) and CaK_{α} X-ray (b) images. Three types of Tfsp can be distinguished: rims with numerous tiny Cpx prisms, irregular crystals and subhedral crystals free of Cpx. Run 5: 1000°C, 25 kbar, with OA. Width of field of view 250 mm. Symbols as in Fig. 1.

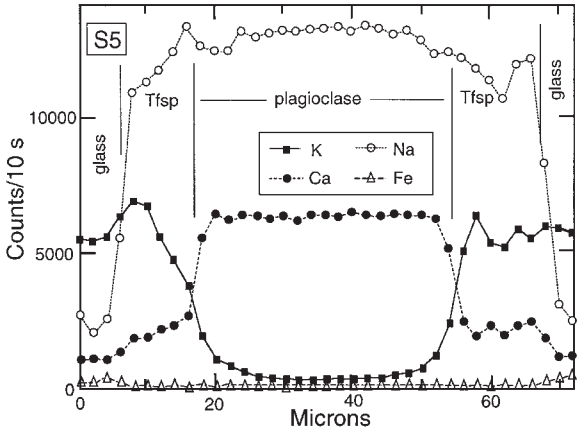

Fig. 9. Compositional profile across a feldspar grain rimmed by ternary feldspar. Ternary feldspar was formed in melting reactions mainly at the expense of plagioclase. Run 5.

Ternary feldspar was observed in all runs with melt proportion from a few percent to ~50 vol. %. Three types of Tfsp grains corresponding to three stages of formation can be distinguished: (1) rims around relict Pl grains (Figs 8 and 10); (2) small, irregular grains (Fig. 8, right lower corner); (3) euhedral and subhedral crystals (Figs 8 and 10). In Fig. 8 all three types of Tfsp grains can be seen. Rims are usually common in samples with a low degree of melting. Although at this stage Tfsp undoubtedly replaces Pl, it was not a simple replacement but rather a melting reaction accompanied by formation of Cpx (see Pl in Fig. 8b); Qtz and Bi were also involved,

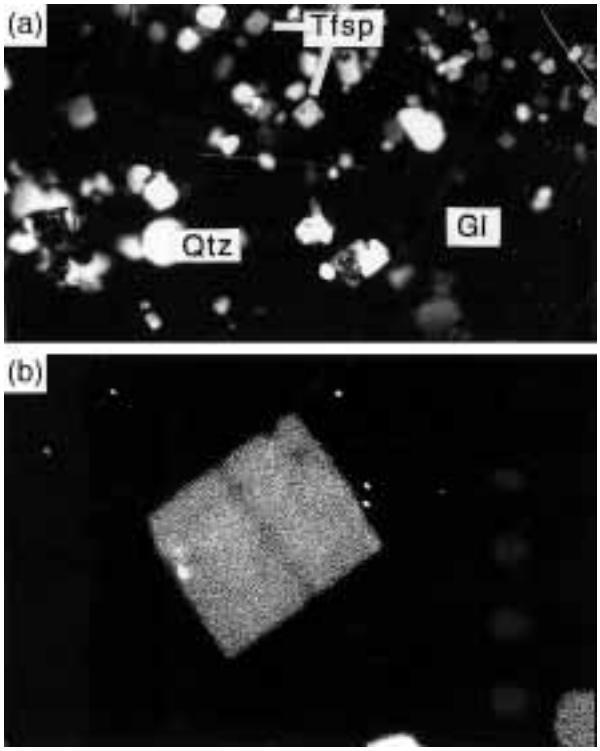

Fig. 10. Euhedral crystals of ternary feldspar in melting experiment with charnockite at 1000°C, 25 kbar, with OA. (a) Cross-polarized light, magnification 250×. (b) CL scanning image, where the line within crystal denotes the scan profile shown in Fig. 11. Long dimension of photograph represents 100 μm.

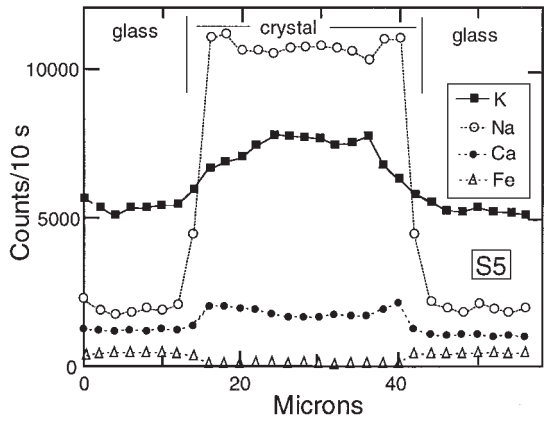

Fig. 11. Compositional profile for K, Na, Ca and Fe across the euhedral crystal of ternary feldspar shown in Fig. 10b.

and Grt was also a reaction product. Figure 9 illustrates the compositional change of a Pl grain in the course of Tfsp formation.

As the degree of melting increases, euhedral crystals of Tfsp predominate (Fig. 10). They are fairly homogeneous (Fig. 11) and, like other phases, are evenly distributed throughout the samples. Interestingly, the Tfsp was formed in melting experiments not only at the expense of plagioclase, but also at the expense of Kfs. As Kfs reacted at the beginning of partial melting, we could not study its transformation in detail. Nevertheless, three main stages were established (Table 5): (1) an increase of albite component in typical relict Kfs grains; (2) rims of Tfsp around Kfs grains; (3) small, irregular Tfsp grains which appear to be relicts of Kfs with compositions close to euhedral Tfsp crystals. The sequence of Tfsp formation is summarized in the Ab–An–Or diagram (Fig. 12), where compositional data from Table 5 for experimentally produced feldspars in the system charnockite–H_2O–CO_2 are plotted. Tfsp appeared with initial melting as shown by Tfsp rims around relict grains of Pl and Kfs from the charnockite. At this stage of melting, the compositions of relict Pl and Kfs depart significantly from their initial compositions. Pl contains up to 10 vol. % of Or component whereas the Ab proportion in Kfs has increased from about 10 to 50 vol. %. This suggests that the formation of Tfsp rims was preceded by diffusion of alkalis within feldspar grains during initial melting. The appearance of Tfsp rims followed by crystallization of euhedral crystals marked an advanced stage of the melting process. The compositional similarity of Tfsp in rims and crystals reflects the increased extent of melting rather than changes in composition. The dispersion of experimental Tfsp data points in Fig. 12 is apparently caused by the broad range of P–T conditions of the runs.

Glass analyses by electron microprobe are given in Tables 3 and 4. The analyses were normalized to anhydrous totals of 100 wt % to facilitate comparisons. Glass compositions are shown in Figs 13 and 14. Perhaps the most striking feature of the glass analyses is their granitic composition irrespective of melting pressure, which ranged from 15 to 25 kbar, and the proportion of melt, which ranged from a few percent to high melting fractions. Although the glass composition clearly changes with temperature, the glass remains granitic up to 80 vol. % melting, and partial melts produced from charnockite at 15, 20 and 25 kbar are all similar in composition (Table 3). Contents of SiO_2 and Al_2O_3 in these melts vary within 1·5–2 wt % whereas other major oxides vary less than 1·5 wt %. Similarly, the proportion of mafic minerals in the norms rarely exceeds 8 wt % and varies less than 5 wt % (Fig. 14). At the same time, a systematic change in the glass composition occurs as the temperature rises (see Fig. 13), as illustrated by discernible increases of MgO and CaO, near-constant FeO*and a decrease in K_2O. An important feature of the partial melts from charnockites is fairly high alkali content, mainly K_2O, best seen at lower and moderate degrees of melting below 50 vol. % and T <1000–1050°C for the system with oxalic acid: 4–5 wt % K_2O and 4–4·5 wt % Na_2O at bulk-rock values of 2·9 and 3·9 wt %, respectively. Interestingly, partial melts produced from fluid-absent melting of charnockite are similar to those obtained in the charnockite–H_2O–CO_2 system (see data in Tables 3 and 4 and in Fig. 14). The only obvious difference is that water-absent melting results in liquids that are richer in the Or component, and in the normative mafic mineral content, by $\sim$1 wt %.

Glasses produced by partial melting of leucogranite (Table 4, Fig. 15) are also granitic, even at 25 kbar, although the amount of SiO_2 (and hence normative Qtz) is lower than in the bulk rock (Table 1, Fig. 15a). As in glasses generated by melting charnockite, glasses derived from leucogranite are significantly enriched in alkalis, which exceed 10 wt %. Reflecting their bulk composition, glasses from leucogranites contain less MgO and CaO. Both leucogranite and charnockite glasses show enhanced Al_2O_3, from 14·5 to 15·5 wt %.

DISCUSSION

Initial melt composition and melting reactions

It was shown above that at all pressures, for both starting materials, the initial melts are granitic. This result is inconsistent with other experiments (Huang & Wyllie, 1975; Johannes & Holtz, 1990; Ebadi & Johannes, 1991) on natural or synthetic Ab–Or–Qtz systems, where the composition of initial melts becomes richer in the feldspar component with increasing pressure. In our experiments, the initial melts (as well as partial melts at higher temperatures) contain 73 $\pm$ 0·5 wt % SiO_2 (Tables 3 and 4).

Table 5: Composition (wt % oxides) and Ab–An–Or proportion for plagioclase, K-feldspar, their reaction products and ternary feldspar in glass; starting material charnockite

	Plagioclase and products of its reactions										
	Initial	Relicts			Zoned grains					Poikilitic micrograins with Cpx microprisms	
					Core		Rim				
SiO_2	61·77	62·15	62·40	61·28	60·95	61·53	64·74	63·26	64·26	65·87	65·45
TiO_2	0·22	0·00	0·00	0·00	0·02	0·06	0·04	0·05	0·06	0·00	0·11
Al_2O_3	23·95	23·97	23·76	23·25	24·69	23·96	19·34	21·92	21·27	21·27	20·02
FeO*	0·03	0·26	0·13	0·08	0·23	0·22	0·09	0·22	0·29	0·16	0·71
MgO	n.d.	n.d.	n.d.	0·02	0·01	0·02	0·02	0·01	0·02	0·00	0·09
CaO	5·75	5·77	5·83	6·13	5·86	5·45	1·81	3·52	2·56	2·12	2·21
Na_2O	8·09	8·20	7·87	7·48	7·28	6·72	7·21	7·64	6·42	8·38	6·43
K_2O	0·22	0·27	0·48	0·49	1·42	2·17	4·89	2·54	5·12	2·66	5·31
Total	100·03	100·62	100·47	98·73	100·46	100·13	98·14	99·16	100·00	100·46	100·33
Ab	70·9	70·9	68·9	66·8	63·5	60·2	63·1	67·9	57·3	74·1	57·7
An	27·8	27·6	28·3	30·3	28·3	27	8·8	17·3	12·6	10·4	11·0
Or	1·3	1·5	2·8	2·9	8·2	12·8	28·2	14·8	30·1	15·5	31·3
Run no.		23	24	54	2	25	5	13	25	24	4

	Micrograins of ternary feldspar in glass						K-feldspar and products of its reactions			
	Irregular micrograins				Euhedral crystals		Rim around Kfs	Relict-looking grains		Initial
SiO_2	64·11	66·65	65·57	65·33	66·28	67·09	64·45	66·52	66·47	65·74
TiO_2	0·02	0·03	0·03	0·04	0·03	0·06	0·02	0·00	0·04	0·03
Al_2O_3	20·91	20·08	20·66	21·56	20·71	19·33	20·77	19·83	19·44	18·20
FeO*	0·30	0·52	0·10	0·19	0·13	0·21	0·15	0·18	0·13	0·01
MgO	0·02	0·23	0·00	0·00	0·00	0·01	0·00	0·00	0·00	0·00
CaO	2·20	1·48	1·93	2·80	1·46	1·13	1·51	1·29	0·78	0·00
Na_2O	8·04	6·30	8·46	6·36	6·94	6·75	7·54	6·18	5·14	1·19
K_2O	3·00	6·01	2·77	4·83	5·33	4·77	4·43	6·44	8·09	14·53
Total	98·60	101·30	99·52	101·11	100·88	99·35	98·87	100·44	100·09	99·70
Ab	71·6	56·9	74·5	57·3	61·6	64·2	66·8	55·5	47·2	11·1
An	10·8	7·4	9·4	14·0	7·2	5·9	7·4	6·4	4·0	0·0
Or	17·6	35·7	16·1	28·7	31·2	29·9	25·8	38·1	48·8	88·9
Run no.	38	24	34	25	24	25	34	3	23	

Decrease of SiO_2 with increasing pressure is seen only in the experiments with leucogranite (Fig. 14) where partial melts for the 25 kbar runs contain 8–9 wt % less normative quartz and more alkali feldspar component than the starting material. However, the amount of SiO_2 in the glass is still >72 wt %. These results are substantiated by melting experiments at 14 and 15 kbar with starting materials more or less chemically similar to charnockite, where initial melts of granitic rather than syenitic composition were observed (Johnston & Wyllie, 1988; Carroll & Wyllie, 1990; Skjerlie & Johnston, 1993). To account for the difference in our results as compared with those obtained in the Ab–Or–Qtz system, specific features of the melting reactions in charnockite need to be analysed.

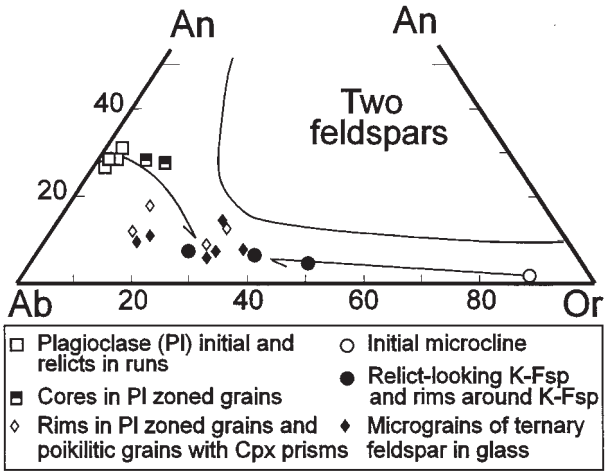

Fig. 12. Experimentally produced feldspars in the charnockite–H_2O–CO_2 system plotted on an Ab–An–Or compositional diagram. Continuous line is isotherm for 1000°C at 10 kbar calculated by Hayob *et al.* (1989). The diagram illustrates various stages of the ternary feldspar formation in the course of melting reactions (see arrows indicating the Pl and Kfs transformation). Chemical data are listed in Table 5.

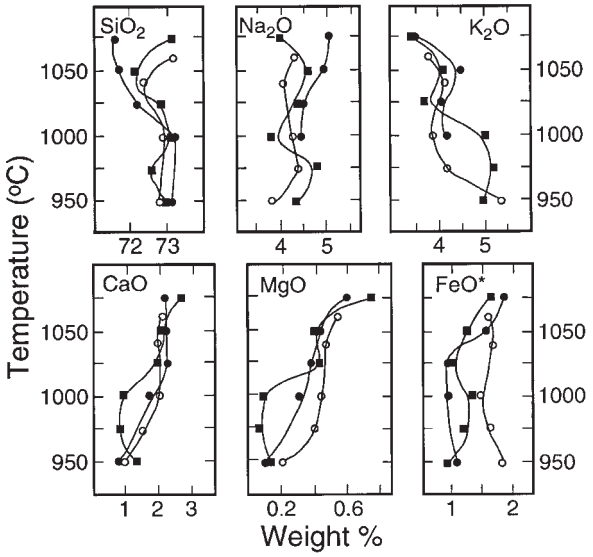

Fig. 13. Major element analyses of quenched melt in the charnockite–H_2O–CO_2 system as a function of temperature and pressure. (For chemical data, see Table 3.) Because of significant loss of Na_2O and K_2O in microprobe analyses of sample from the 20 kbar, 950°C run, these data were not used. Symbols as in Figs 4 and 6.

The character of melting reactions is clearly seen in the fluid-absent runs when the melt fraction is <10 vol. %. The first melt portion (Fig. 3a) occurred around pseudomorphic aggregates of garnet replacing biotite. The analysis of glass and crystal phases around these garnet aggregates showed that both quartz and plagioclase were involved in the melting reaction. Relict quartz grains are either corroded or overgrown by rims of later quartz creating euhedral grains. Plagioclase crystals consist of a twinned plagioclase core surrounded by Tfsp rims that in turn incorporate numerous tiny prisms of cpx (Fig. 8). Small grains of Tfsp and cpx are also present within pools of glass. These observations suggest that the melting reaction in the fluid-absent melting experiments is

$$\text{Bi} + \text{Pl} + \text{Qtz} (+ \text{Hbl}) = \text{Grt} + \text{Cpx} + \text{Tfsp} + \text{L}. \quad (1)$$

In runs with oxalic acid the initial melt production was accompanied by formation of the same mineral assemblage, but because of the free fluid in the system, melt reactions were not confined to biotite grains; melting started at much lower temperature and occurred throughout the sample (see Fig. 3b). Consequently, Kfs and Opx were also involved in the melting reaction:

$$\text{Bi} + \text{Pl} + \text{Kfs} + \text{Qtz} + \text{Hbl} + \text{Opx} + \text{H}_2\text{O} = \text{Grt} + \text{Cpx} + \text{Tfsp} + \text{L}. \quad (2)$$

Reactions (1) and (2) demonstrate incongruent melting of charnockite as distinct from congruent melting in the Ab–Or–Qtz system. In addition to melt, the peritectic melting reactions formed Grt and Cpx containing about 40 and 50 wt % SiO_2, respectively, and Tfsp with 65 wt % SiO_2, all containing less SiO_2 than the starting material (see Tables 1 and 3–5). Consequently, the melt is enriched in SiO_2 both at the initial and more evolved stages. The greater the Ca, Mg and Fe content of the source rock, the more Grt and Cpx will form, and the more silica in the initial melt. Partial melting of leucogranite that is rather close in chemical composition to the Ab–Or–Qtz system resulted in production of a less silicic and more alkali-rich initial melt compared with the starting material (Table 4, Fig. 14). However, because of the presence of 2·5 wt % CaO, FeO and MgO, Cpx and Grt were also formed, limiting the generation of syenitic initial melt.

These data suggest that partial melting of common natural silicic rocks at very high pressure, from 15 to 25 kbar, does not give rise to syenite magmas. This is a direct result of incongruent melting reactions and the formation of low-silica minerals (Grt, Cpx), which enrich the initial melts in SiO_2 to give a granitic composition.

The role of ternary feldspar in buffering partial melt composition

It was shown above that during melting, garnet, clinopyroxene and feldspar entered the melt as temperature rose. Grt persists throughout the entire melting interval, and in runs with charnockite it comprises ~15–17 vol. %. Cpx also persists through a wide range of temperature, but decreases noticeably when the degree of melting

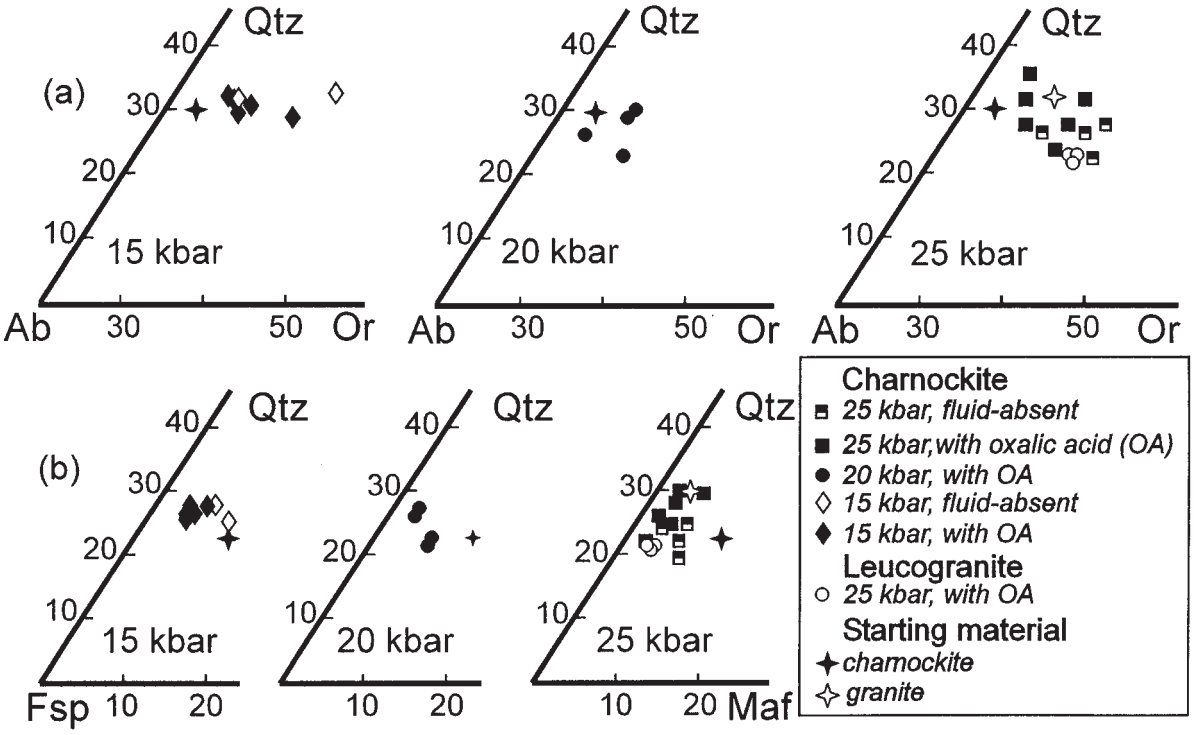

Fig. 14. Composition of experimentally produced glasses plotted on the triangles (a) albite–orthoclase–quartz (Ab–Or–Qtz) and (b) feldspar–quartz–mafic minerals (Fsp–Qtz–Maf).

exceeds 50–60 vol. %, and is absent at 80–85 vol. % of melt. Ternary feldspar, like Grt and Cpx, appears at the very beginning of melting and disappears at ~50 vol. % melting.

Regular change of the chemical composition of melt and crystal phases occurs with temperature rise at all pressures: garnets become enriched in MgO (pyrope) whereas the content of FeO decreases (Figs 4 and 5); pyroxenes show an increase of MgO and CaO, and decrease of Na_2O and Al_2O_3 (Figs 6 and 7); ternary feldspar is enriched in Or, less in An (Fig. 12). The melt composition remains fairly constant up to temperatures of 1000–1025°C, which correspond to ~50 vol. % melting, although K_2O systematically decreases from ~5 to 4 wt % whereas CaO and MgO increase slightly, in the range of 1 wt % and 0·3 wt %, respectively (Fig. 13). At higher temperatures and hence melting beyond 50%, the variation curves of K_2O, MgO, FeO*and SiO_2 show different trends, reflecting an abrupt change of the melt composition corresponding to the disappearance of ternary feldspar.

The above observations provide constraints for melt development with the onset of melting described by equations (1) and (2). Additional melting is accompanied by regular changes in the Grt and Cpx compositions and consumption of Tfsp by melting reactions. In the course of reactions, Grt and Cpx form and act as sinks for refractory elements (Mg, Ca) whereas less refractory Na, Fe and Al are concentrated in the melt (Figs 4 and 6). These trends agree with our understanding of the limited solubility of ferromagnesian phases in silicic melts (Clemens & Wall, 1981; Naney, 1983; Puziewicz & Johannes, 1988). The main crystalline host of alkalis is Tfsp, containing 55–70 wt % Ab and 15–30 wt % Or (Table 5). As temperature rises, the proportion of Tfsp decreases, whereas K_2O in Tfsp increases (see Fig. 12). Relict quartz grains that persist up to 80 vol. % of melting serve as a source of silica. The melting reaction at this stage is

$$\text{Tfsp} + \text{Qtz} + \text{Grt1} + \text{Cpx1} + \text{L1} = \text{Grt2} + \text{Cpx2} + \text{L2} \quad (3)$$

where Grt2 and Cpx2 are minerals enriched in refractory constituents (see above) and equilibrated with new melt L2.

Thus, ternary feldspar and relict Qtz buffer the melt composition and extend its relative compositional stability to ~50 vol. % melting. Similarly, K-rich plagioclase had been noted in earlier melting experiments using biotite-bearing tonalite with a composition similar to our charnockite (Skjerlie & Johnston, 1993): at 10 kbar and 1025–1050°C the feldspathic phase contains 1·6–1·7 wt % K_2O and ~5·2–5·5 wt % CaO.

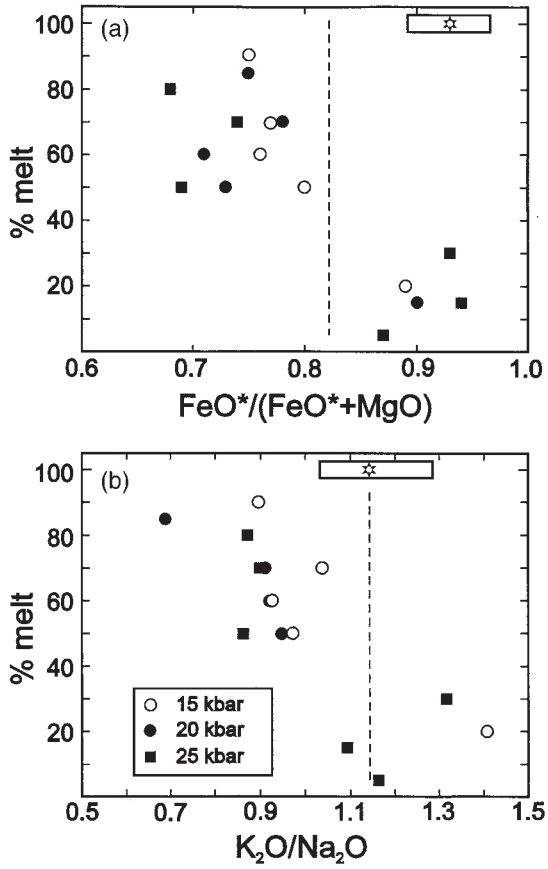

Fig. 15. Compositional variation of quenched melt in the charnockite–H_2O–CO_2 system plotted as FeO*/(FeO* + MgO) vs % melt (a), and K_2O/Na_2O vs % melt (b). Vertical dashed lines: (a) lower limit of FeO*/(FeO* + MgO) ratio in the A-type granites with 72 wt % SiO_2 [after Anderson & Morrison (1992)]; (b) value of K_2O/Na_2O in the average A-type granite (Whalen *et al.*, 1987). Asterisk and rectangle near the upper right corner: average A-type granite (Whalen *et al.*, 1987) and compositional range of Late Palaeozoic A-type granites in Transbaikalia (Zanvilevich *et al.*, 1985; Wickham *et al.*, 1995), respectively.

At higher degrees of melting, Cpx with relict Qtz enters the melt at temperatures from 975 to 1025°C, depending on pressure (Fig. 2). As a consequence, the melt becomes enriched in Ca, Mg and Fe, and depleted in K_2O but with near-constant silica (Fig. 14). At the same time, Na_2O remains high until Cpx, the source of sodium in melting reactions at this stage, is consumed. A granitic glass composition is retained even at very high degrees of melting, ~80 vol. % (Figs 13 and 14), maintained by the low silica content in Cpx and Grt. We thus conclude that partial melting of silicic rocks of granite and quartz monzonite compositions at depths where pressure is >15 kbar will result in melts of granitic composition, even to high degrees of melting.

Effect of oxalic acid addition on the composition of melting reaction products

As most experiments were performed with oxalic acid added, we compared these results with the fluid-absent data. To produce the same amount of melt, fluid-absent melting requires 150–170°C higher temperatures than melting with OA (Table 2). Despite this temperature difference, the mineral assemblages in both are identical. The compositions of garnet and clinopyroxene are also similar (Figs 5 and 7), and melt compositions differ very little (Fig. 14, Tables 3 and 4). A slight increase of mafic components in water-absent partial melts (Fig. 14) was caused by the increased solubility of ferromagnesian phases at higher temperatures. These experiments suggest that the presence of H_2O and CO_2 did not greatly affect the compositions of phases in the melting reactions. Rather, H_2O in H_2O–CO_2 fluid lowers the melting temperature as compared with the volatile-free system. The presence of H_2O and CO_2 is responsible for the low analysis totals of ~94 wt % for runs with 70–80 vol. % of melt (Table 3).

Restite separation

Two specific features are characteristic of melting at high pressure:

(1) typical granitic liquids are produced by melting of the quartzofeldspathic source rock up to 50–60 vol. %, i.e. large-scale melting.

(2) The residual mineral assemblage consists of garnet, clinopyroxene, relict quartz and possibly minor ternary feldspar.

In a magma containing ~35–40 vol. % of Grt and Cpx crystals, removal of these residual solid phases (restite segregation) may be the dominant process leading to the accumulation of large volumes of homogeneous granitic liquid. This is possible because mafic minerals are denser than the host melt by a factor of 1·4–1·9, and would have a strong tendency to settle. Less dense grains of relict Qtz and Tfsp would not readily settle; instead, these minerals would enter the melt during its ascent as pressure decreases. Some important consequences follow from this scenario:

(1) the granitic magma may evolve to be practically devoid of residual crystal phases, and this is indeed one of the most striking features of many postcollision granites (Zanvilevich *et al.*, 1985).

(2) As Grt and Cpx are the main phases removed from the melt, their fractionation would deplete the melt in heavy rare earth elements (REE) and give a heavy REE (HREE)-depleted pattern in the resulting granite. Some fractionation of feldspar in the course of magma ascent to higher levels could provide negative Eu anomalies. These features are characteristic of many granites, including A-type granites (Whalen *et al.*, 1987; Eby, 1990).

(3) Our experiments suggest that silicic melt produced at great depth would be in equilibrium with Grt and thus would be subaluminous to peraluminous, even when source rocks are metaluminous.

Restite separation may complicate relationships between a silicic melt layer and a basaltic magma heat source underplated beneath it. In recent years, the idea of silicic magma generation above basalt intrusions underplated or intraplated with respect to crustal terrane has become popular (Huppert & Sparks, 1988; Harley, 1989; Vielzeuf *et al.*, 1990; Litvinovsky & Podladchikov, 1993). If this process occurred at great depth, at a pressure >15 kbar, Grt and Cpx would settle through the silicic layer to the basalt reservoir surface. Two possible scenarios can be pictured: (1) the basalt layer was sufficiently viscous that settling crystals were accumulated immediately above its upper surface; (2) convective stirring within the basalt reservoir (Litvinovsky & Podladchikov, 1993) caused Grt and Cpx crystals to mingle with the basalt. At this depth, basalt magma would crystallize to an eclogite mineral assemblage (i.e. a Grt + Cpx assemblage). Eclogite would contain Grt and Cpx derived from the basalt, and also Grt and Cpx that had separated from the silicic melt.

Fluid-absent melting vs melting in an open system

Our experiments demonstrate that fluid-absent melting (~50–60 vol. %) occurs at ~1150–1200°C. This temperature is anomalously high as it is comparable with the subliquidus temperature of basalt magmas with 2 wt % H_2O at high pressure (Stern & Wyllie, 1978; Huang & Wyllie, 1986). The water content in our fluid-absent experimental melts was at most 1·5 wt %. In addition, natural source rocks should lose most biotite in the course of prograde metamorphism to eclogite grade, and the real amount of water in the derived melt could be <1·5 wt %.

Runs with OA to give 2 wt % H_2O and ~3 wt % CO_2 showed that ~50–60% melting at 15–25 kbar pressure occurred within the range 975–1050°C (Table 2). Under these conditions, the silicic melt is water undersaturated (~4 wt % H_2O) but the temperatures are more realistic. This suggests that if granite magma forms at great depth, melting in the presence of a CO_2–H_2O fluid is the more plausible scenario. The possible fluid source could be an underplated basalt reservoir (Litvinovsky, 1993; Litvinovsky & Podladchikov, 1993).

Implication for the generation of A-type granites

The above results demonstrate that melting of charnockite and granite at pressures >15 kbar results in a granitic rather than syenitic melt. For melting from a few percent to ~50%, the melt composition is relatively constant and is characterized by rather high K_2O, Na_2O and FeO/MgO, and low MgO and CaO (Tables 3 and 4, Figs 13 and 14). These compositional features of partial melts allow us to compare them with A-type granites (Whalen *et al.*, 1987; Eby, 1990; Anderson & Morrison, 1992). Absence of trace element data prevents detailed comparisons, therefore we have to restrict discussion to major element composition only. In Fig. 15 the experimental data are plotted on diagrams FeO*vs percent melt and K_2O/Na_2O vs percent melt. Also plotted are the average A-type granite composition (by Whalen *et al.*, 1987) as well as average Late Palaeozoic A-type granites from the Transbaikalian province (our data). One can see that only those melts that were produced by melting <30–40% correspond to A-type granite magmas, and even these experimental melts contain ~1 wt % more Al_2O_3. Thus, the assumption that a significant amount of A-type granite magma could be produced at very great depth by partial melting of quartzofeldspathic rocks of granodiorite, quartz monzonite or K-rich tonalite composition is only partly supported by our experimental data.

It is well known that many A-type granites have isotopic characteristics indicating significant involvement of mantle material (Barker *et al.*, 1975; Wickham *et al.*, 1995; Zhao *et al.*, 1995). There is also geological evidence that cannot be explained in the context of a crustal origin of all A-type granites; specifically, the problem of the origin of syenite magmas genetically linked to A-type granites. Syenites are present in many A-type granitoid suites throughout the world, although usually in small volumes (Eby, 1990). However, syenites may dominate, as in Transbaikalia (Zanvilevich *et al.*, 1985); moreover, it is possible that syenite magma in some cases was parental to the granitic melt (Zanvilevich *et al.*, 1995). Our experimental data demonstrate that a syenite melt cannot be produced by partial melting of common quartzofeldspathic rocks even at very high pressure, and that other models must therefore be explored. A two-stage model (Wickham *et al.*, 1995) has been proposed: (1) mixing of silicic melt with underplated alkali-rich basalt magma to form a hybrid monzonite melt; (2) fractional crystallization of this hybrid magma to give syenite, and then granite residual melts (partial melting of hybrid monzonite would also produce syenite melt). Such a model of deep crustal melting seems reasonable, as it is probable that a high proportion of the silicic melt would hybridize with underplated basalt magma or with products of its differentiation. In the future it is important to distinguish A-type granitoids of crustal from those of hybrid mantle–crustal origin.

CONCLUSION

(1) Partial melting of natural quartzofeldspathic rocks at high pressure, from 15 to 25 kbar, produces granitic melt with 72–73 wt % SiO_2. Unlike melting in the pure Ab–Or–Qtz system, high-pressure melting of natural rocks does not produce silica-poor syenitic or quartz syenitic initial melt. This is because partial melting in the ideal Ab–Or–Qtz system is congruent, whereas in rocks containing significant Mg and Fe, melting is incongruent and is accompanied by the formation of the low-silica mafic minerals garnet and clinopyroxene. The excess SiO_2 enters the melt and makes it granitic rather than syenitic. Syenitic liquids cannot be produced by partial melting of quartzofeldspathic rocks containing significant Mg and Fe, even at high pressures.

(2) The composition of partial melts produced from charnockite at high pressure is granitic to as much melting as 50–60 vol. %. This is caused by the buffering role of ternary feldspar that usually forms, along with garnet and pyroxene, at the very beginning of melting. At more evolved stages of melting, Tfsp enters the melt together with restitic quartz, and the melt remains granitic until ternary feldspar is consumed.

(3) When the extent of melting exceeds 50 vol. % (at 975–1025°C, depending on pressure), clinopyroxene (also with residual quartz) enters the melt, which accordingly becomes more Ca and Mg rich, and contains less potassium. However, a granitic melt composition is retained to degrees of melting of 75–80 vol. % because low-silica garnet and pyroxene are the only restite phases. This suggests that at great depth, partial melting of source rocks corresponding in composition to granite, quartz monzonite or biotite-rich tonalite could produce granitic melts up to very high degrees of melting.

(4) When the melt fraction exceeds 50–60 vol. %, the problem of melt segregation becomes a problem of restite separation from the melt. At great depth the restite consists of garnet and clinopyroxene, so that density-driven separation of crystals from high-silica silicic melt would readily occur and result in the accumulation of large volumes of granite magma, almost entirely devoid of residual crystals. Granites formed in this way would be characterized by HREE-depleted REE element pattern.

(5) Granite magmas produced at great depth will be in equilibrium with garnet and consequently could become subaluminous or peraluminous even if the source rocks were metaluminous.

ACKNOWLEDGEMENTS

This study was partly supported by grants from the Soros International Science Foundation (RNU 000 and RNU 3000) and the Russian Foundation of Basic Researches (96-05-64027 and 97-05-96355) to B.A.L. Support for I.M.S. was from NASA NAGW 3416 and NSF EAR 96-27336, and instrumental support was from NSF EAR 93-03530 and EAR 93-16062. Experimental facilities in the Department of Geophysical Sciences (University of California) were supported by NSF grant EAR 93-10264 to R. C. Newton. We are greatly indebted to Professor Newton for his close collaboration and guidance in experiments, and we would like to thank A. N. Zanvilevich, B. Groshau and M. Slagel for invaluable aid in experimental work and data processing. The manuscript had been substantially improved after thorough reviews by K. P. Skjerlie and J. L. Anderson.

REFERENCES

Andersen, T., Austrheim, H., Burke, E. A. J. & Elvevold, S. (1993). N_2 and CO_2 in deep crustal fluids; evidence from the Caledonides of Norway. *Chemical Geology* **108**, 113–132.

Anderson, J. L. & Morrison, J. (1992). The role of anorogenic granites in the Proterozoic crustal development of North America. *Developments in Precambrian Geology* **10**, 263–299.

Aranovich, L. Ya., Shmulovich, K. I. & Fed'kin, V.V. (1987). The H_2O and CO_2 regime in regional metamorphism. *International Geology Review* **29**, 1379–1401.

Barbey, P., Macaudiere, J. & Nzenti, J. P. (1990). High-pressure dehydration melting of metapelites: evidence from migmatites of Yaounde (Cameroon). *Journal of Petrology* **31**, 401–427.

Barker, F., Wones, D. R., Sharp, W. N. & Desborough, G. A. (1975). The Pikes Peak Batholith, Colorado Front Range, and a model of the origin of the gabbro–anorthosite–syenite–potassic granite suite. *Precambrian Research* **2**, 97–160.

Black, P. M., Brothers, R. N. & Yokoyama, K. (1988). Mineral parageneses in eclogite-facies meta-acidites in northern New Caledonia. In: Smith, D. C. (ed.) *Eclogites and Eclogite-facies Rocks: Developments in Petrology, 12*. Amsterdam: Elsevier, pp. 271–290.

Carroll, M. R. & Wyllie, P. J. (1990). The system tonalite–H_2O at 15 kbar and genesis of calc-alkaline magmas. *American Mineralogist* **75**, 345–357.

Clemens, J. D. & Wall, V. J. (1981). Origin and crystallization of some peraluminous (S-type) granitic magmas. *Canadian Mineralogist* **19**, 111–131.

Clemens, J. D., Collins, W. J., Beams, S. D., White, A. J. R. & Chappell, B. W. (1982). Nature and origin of A-type granites with particular reference to Southeastern Australia. *Contributions to Mineralogy and Petrology* **80**, 189–200.

Clemens, J. D., Holloway, J. R. & White, A. J. R. (1986). Origin of an A-type granite: experimental constraints. *American Mineralogist* **71**, 317–324.

Collerson, K. D. & Fryer, B. J. (1978). The role of fluids in the formation and subsequent development of early continental crust. *Contributions to Mineralogy and Petrology* **67**, 151–167.

Creaser, R. A., Price, R. C. & Wormald, R. J. (1991). A-type granites revisited: assessment of a residual-source. *Geology* **19**, 163–166.

Ebadi, A. & Johannes, W. (1991). Beginning of melting and composition of first melts in the system Qz–Ab–Or–H_2O–CO_2. *Contributions to Mineralogy and Petrology* **106**, 286–295.

Eby, G. N. (1990). The A-type granitoids: a review of their occurrence and chemical characteristics and speculations on their petrogenesis. *Lithos* **26**, 115–134.

Grew, E. S. (1984). A review of Antarctic granulite-facies rocks. *Tectonophysics* **105**, 177–191.

Harley, S. L. (1989). The origin of granulites: a metamorphic perspective. *Geological Magazine* **126**, 215–247.

Hayob, J. L., Essene, E. J., Ruiz, J., Ortega-Guitiérrez, F. & Aranda-Gómez, J. J. (1989). Young high-temperature granulites from the base of the crust in central Mexico. *Nature* **342**, 265–268.

Huang, W. L. & Wyllie, P. J. (1975). Melting reactions in the system $NaAlSi_3O_8$–$KAlSi_3O_8$–SiO_2 to 35 kilobars, dry and with excess water. *Journal of Geology* **83**, 737–748.

Huang, W. L. & Wyllie, P. J. (1981). Phase relationships of S-type granite with H_2O to 35 kbar: muscovite granite from Harney Peak, South Dakota. *Journal of Geophysical Research* **86**, 10515–10529.

Huang, W. L. & Wyllie, P. J. (1986). Phase relationships of gabbro–tonalite–granite–water at 15 kbar with applications to differentiation and anatexis. *American Mineralogist* **71**, 301–316.

Huppert, H. E. & Sparks, R. S. J. (1988). The generation of granitic magmas by intrusion of basalt into continental crust. *Journal of Petrology* **29**, 599–624.

Johannes, W. & Holtz, F. (1990). Formation and composition of H_2O-undersaturated granitic melts. In: Ashworth, J. R. & Brown, M. (eds) *High-temperature Metamorphism and Crustal Anatexis*. London: Unwin Hyman, pp. 87–104.

Johnston, A. D. & Wyllie, P. J. (1988). Constraints on the origin of Archean trondhjemites based on phase relationships of Nûk gneiss with H_2O at 15 kbar. *Contributions to Mineralogy and Petrology* **100**, 35–46.

Litvinovsky, B. A. (1990). Anomalously high temperatures of generation of silicic magmas in active mobile belts. *Transactions (Doklady) of USSR Academy of Sciences: Earth Science Sections* **310**, 129–131.

Litvinovsky, B. A. (1993). Water–carbon dioxide fluids in the lower and middle crust: role in magma generation and metamorphism. *Doklady RAS* **332**, 75–78 (in Russian).

Litvinovsky, B. A. & Podladchikov, Yu. Yu. (1993). Crustal anatexis during the influx of mantle volatiles. *Lithos* **30**, 93–107.

Litvinovsky, B. A., Gordienko, I. V. & Zanvilevich, A. N. (1989). The evolution of Late Paleozoic plutonic magmatism and volcanism of Transbaikalia and Mongolia. In: Ichikawa, K. (ed.) *Report 4 of the IGCP Project 224: Pre-Jurassic Evolution of Eastern Asia*. Osaka: Osaka Institute of Technology, pp. 135–142.

Naney, M. T. (1983). Phase equilibria of rock forming ferromagnesian silicates in granitic systems. *American Journal of Science* **283**, 993–1033.

Newton, R. C., Smith, J. V. & Windley, B. F. (1980). Carbonic metamorphism, granulites and crustal growth. *Nature* **288**, 45–50.

Patiño Douce, A. E. P. & Johnston, A. D. (1991). Phase equilibria and melt productivity in the pelitic system: implications for origin of peraluminous granitoids and aluminous granulites. *Contributions to Mineralogy and Petrology* **107**, 202–218.

Petrova, Z. I. & Levitsky, V. I. (1984). *Petrology and Geochemistry of Granulite Complexes in Pribaikalia*. Novosibirsk: Nauka, 198 pp. (in Russian).

Pin, Ch. & Vielzeuf, D. (1988). Les granulites de haute-pression d'Europe moyenne témoins d'une subduction éo-hercynienne. Implications sur l'origine des groupes leptyno-amphiboliques. *Bulletin de la Société Geologique de France* **1**, 3–20.

Puziewicz, J. & Johannes, W. (1988). Phase equilibria and compositions of Fe–Mg–Al minerals and melts in water-saturated peraluminous granitic systems. *Contributions to Mineralogy and Petrology* **100**, 156–168.

Rämö, O. T. (1991). Petrogenesis of the Proterozoic rapakivi granite and related basic rocks of southeastern Fenoscandia: Nd and Pb isotopic and general geochemical constraints. *Bulletin of the Geological Survey of Finland* **355**, 161 pp.

Sandiford, M. & Powell, R. (1986). Pyroxene exolution in granulites from Fyfe Hills, Enderby Land, Antarctica: evidence for 1000°C metamorphic temperatures in Archean continental crust. *American Mineralogist* **71**, 946–954.

Schertl, H. P., Schreyer, W. & Chopin, C. (1991). The pyrope–coesite rocks and their country rocks at Parigi, Dora Maira Massif, Western Alps: detailed petrography, mineral chemistry and *PT*-path. *Contributions to Mineralogy and Petrology* **108**, 1–21.

Schliestedt, M. & Okrusch, M. (1988). Meta-acidites and silicic metasediments related to eclogites and glaucophanites in northern Sifnos, Cycladic Archipelago, Greece. In: Smith, D. C. (ed.) *Eclogites and Eclogite Facies Rocks: Developments in Petrology, 12*. Amsterdam: Elsevier, pp. 291–334.

Schmidt, M. W. (1993). Phase relations and compositions in tonalite as a function of pressure: an experimental study at 650°C. *American Journal of Science* **293**, 1011–1060.

Schreyer, W. (1988). Subduction of continental crust to mantle depths: petrological evidence. *Episodes* **11**, 97–104.

Schreyer, W., Massonne, H. J. & Chopin, C. (1987). Continental crust subducted to depths near 100 km: implications for magma and fluid genesis in collision zones. In: Mysen, B. O. (ed.) *Magmatic Processes: Physicochemical Principles. Geochemical Society, Special Publication* **1**, 155–163.

Skjerlie, K. P. & Johnston, A. D. (1993). Fluid-absent melting behavior of an F-rich tonalitic gneiss at mid-crustal pressures: implications for the generation of anorogenic granites. *Journal of Petrology* **34**, 785–815.

Skjerlie, K. P. & Johnston, A. D. (1996). Vapour-absent melting from 10 to 20 kbar of crustal rocks that contain multiple hydrous phases: implications for anatexis in the deep to very deep continental crust and active continental margins. *Journal of Petrology* **37**, 661–691.

Snoeyenbos, D. R. & Williams, M. L. (1994). An Archean eclogite facies terrane from the Snowbird tectonic zone, Northern Saskatchewan. *EOS Supplement, 1994 Spring Meeting Abstracts*, 355.

Sobolev, N. V., Dobretsov, N. L., Bakirov, A. B. & Shatsky, V. S. (1986). Eclogites from various types of metamorphic complexes in the USSR and problems of their origin. *Geological Society of America, Memoir* **164**, 349–363.

Stern, C. R., Huang, W.-L. & Wyllie, P. J. (1975). Basalt–andesite–rhyolite–H_2O: crystallization intervals with excess H_2O and H_2O-undersaturated liquidus surfaces to 35 kilobars, with implications to magma genesis. *Earth and Planetary Science Letters* **98**, 189–196.

Stern, C. R. & Wyllie, P. J. (1978). Phase compositions through crystallization intervals in basalt–andesite–H_2O at 30 kbar with implications for subduction zone magmas. *American Mineralogist* **63**, 641–663.

Touret, J. L. R. (1992). CO_2 transfer between the upper mantle and the atmosphere; temporary storage in the lower continental crust. *Terra-Nova* **4**, 87–98.

Vielzeuf, D. & Holloway, J. R. (1988). Experimental determination of the fluid-absent melting relations in the pelitic system. *Contributions to Mineralogy and Petrology* **98**, 257–276.

Vielzeuf, D., Clemens, J. D., Pin, C. & Moinet, E. (1990). Granites, granulites, and crustal differentiation. In: Vielzeuf, J. D. & Vidal, Ph. (eds) *Granulites and Crustal Evolution. Series C: Mathematical and Physical Sciences, 311*. Dordrecht: Kluwer Academic, pp. 59–85.

Whalen, J. B., Currie K. L. & Chappell, B. W. (1987). A-type granites: geochemical characteristics, discrimination, and petrogenesis. *Contributions to Mineralogy and Petrology* **95**, 407–419.

Wickham, S. M., Litvinovsky, B. A., Zanvilevich, A. N. & Bindeman, I. N. (1995). Geochemical evolution of Phanerozoic magmatism in Transbaikalia, East Asia: a key constraint on the origin of K-rich silicic magmas and the process of cratonization. *Journal of Geophysical Research* **100**, 15641–15654.

Zanvilevich, A. N., Litvinovsky, B. A. & Andreev, G. V. (1985). *Mongolian–Transbaikalian Alkaline Granitoid Province*. Moscow: Nauka, 232 pp. (in Russian).

Zanvilevich, A. N., Litvinovsky, B. A., Wickham, S. M. & Bea, F. (1995). Genesis of alkaline and peralkaline syenite–granite series: the Kharitonovo pluton (Transbaikalia, Russia). *Journal of Geology* **103**, 127–145.

Zhang, R. Y., Liou, J. G. & Cong, B. (1994). Evidence of supercrustal rock subducted to mantle depths: coesite-bearing jadeite quartzite from Dabie UHP Terrane, central China. *EOS Supplement, 1994 Spring Meeting Abstracts*, 355.

Zhao, J. X., Shiraishi, K., Ellis, D. J. & Sheraton, J. W. (1995). Geochemical and isotopic studies of syenites from the Yamato Mountains, East Antarctica: implications for the origin of syenitic magmas. *Geochimica et Cosmochimica Acta* **59**, 1363–1382.